BOYD TRUSTED INNOVATION

SiC MOSFET-Based High Performance Double Side Cooled Module and Compact Cooler for High Power-Density Automotive Inverter Applications

Ajay Poonjal Pai[1], Alex Widhalm[2], Michael Ebli[2], Matthias Kurz[2], Marco La Foresta[3], Marina Fernández Osorio[3] [1]Infineon Technologies AG, Am Campeon 1-15, 85579 Neubiberg, Germany. AjayPoonjal.Pai@Infineon.com [2]Infineon Technologies AG, Max-Planck-Str. 5, 59581 Warstein, Germany.
[3]Boyd Bologna Srl, Via del Fonditore 4, 40138 Bologna, Italy. Marco.LaForesta@boydcorp.com, Marina.Fernandez@boydcorp.com

Abstract— **This paper presents a high performance Double Side Cooled (DSC) module based on trench Silicon Carbide (SiC) MOSFETs, and demonstrates the design of an optimized cooler. The cooler's thermal performance is simulated and experimentally verified. The static and switching characteristics of the SiC module are experimentally characterized and compared against a Silicon- (Si) based DSC Module to determine the benefits of SiC at the module and inverter levels.**

Keywords— Silicon Carbide MOSFET, Automotive Traction Inverter, Double Side Cooled Power Module, Cooler Design

I. Introduction

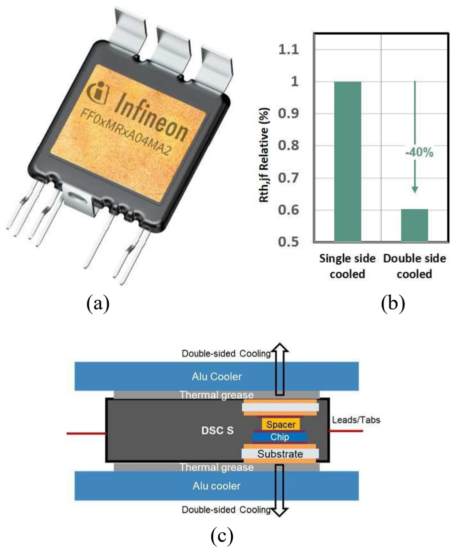

Fig. 1 (a) Infineon's HybridPACK™ DSC module, (b) Simulation result showing that DSC module offers 40% lower $R_{th,jf}$ than a single side cooled module with the same footprint [1], (c) DSC thermal stack.

Infineon's HybridPACK™ DSC Power Module equipped with CoolSiC™ Trench Silicon Carbide (SiC) MOSFETs (see Fig. 1 (a)) have been shown to offer significant benefits at the module and inverter levels [1]. Fig. 1 (b) shows that the simulated junction-fluid thermal resistance $R_{th,jf}$, of a DSC module can be reduced by 40% compared to a single side cooled module with the same footprint and under the same boundary conditions [1]. This would translate into a higher current capability, I_{RMS} which is particularly important for semiconductors such as SiC, which are known to be materially more expensive than Silicon (Si). Fig. 1 (c) shows the thermal stack of the DSC, which has been demonstrated in [1] to offer superior performance. The DSC is an indirect-cooled module, and optimization of the module alone is not sufficient. It is necessary to optimize the cooler and the Thermal Interface Material (TIM) as well. This paper presents a BOYD™ aluminum cooler, specially designed and optimized for the
DSC module and its thermal/hydraulic simulation results are discussed. This cooler is then experimentally characterized and compared against the simulation results. Furthermore, the module is also characterized in a lab setup cooler to further understand its thermal performance. To deduce the powerloss benefits of the SiC DSC module, it is experimentally compared against a comparable Si DSC module, and simulations are performed to confirm efficiency benefits at the system level.

II. Design of a Compact Aluminium Cooler for DSC

This section discusses the design of an aluminum-based application-near BOYD™ cooler structure for the DSC module. The cooler is kept as compact as possible, to reach a high level of power density. The double side cooling structure includes two Liquid Cold Plates (LCP) as shown in Fig. *2* (a), along with the exploded views of the top LCP (Fig. *2* (b)). Both LCPs share the same geometry regarding number of layers, inlet/outlet connectors, channel structure, turbulator and perimeter shape. Each LCP includes a *top layer* with the location for the inlet/outlet hydraulic connectors, a *channel layer* with the location of the turbulator and a *bottom layer* to close the channel path. The TOP LCP includes two additional hydraulic connectors, in order to divide the fluid flow rate equally on both top and bottom. All interfaces between the top and bottom LCPs are sealed with O-rings. All layers are obtained by laser cut, the connectors by lathing and the turbulators by stamping. Two steel plates are added on top and bottom to compensate the bending effect during the assembling process, which might reduce the contact surface between the LCPs and the central SiC module. Fig. *2* (c) shows the cooler after integrating the DSC modules, indicating the dimensions relevant for the cooler. It can be seen that the cooling structure combined with the module is very compact and occupies a volume of only 0.4 L as per the dimensions defined in the figure. For benchmarking the cooling performance, it would be relevant to neglect the volume of the module not in contact with the cooler, and the volume in this case is 0.12 L, paving the way for a high power density. The fabricated cooler is shown in Fig. 3.

A. Thermal and Hydraulic CFD Simulation of the Cooler

A Computational Fluid Dynamics (CFD) simulation is run in Boyd SmartCFD to predict the thermal and hydraulic performance of the cooler. The complete internal structure of the module is implemented to calculate an accurate thermal distribution. The overview of the simulated geometry is shown in Fig. 4 and the boundary conditions are summarized in Table *1*. Two modules (A and B) with different chip content are investigated. Detailed full Navier-Stokes CFD Solver is chosen for the flow-simulation considering a turbulent flow regime. Finite volume discretization is applied to represent both the solid and fluid. As the geometry is regular, particularly in the finned area, the geometry is simplified into hexahedral blocks and a hexahedral mesh is used to represent the geometry for the most accurate calculation of the behavior of fluid in contact with the cooler fins. For brevity, the metallic surfaces are assumed to be flat and the TIM has been modelled as a homogenous layer of uniform thickness between the metallic surfaces.

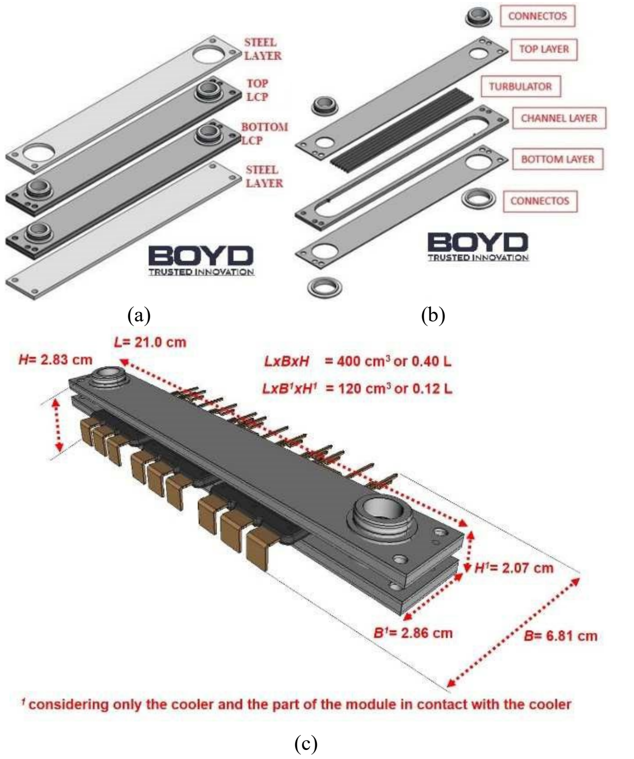

Fig. 2 The designed cooling structure for the DSC modules, showing (a) the top and bottom LCP with the steel plates to compensate bending effects during assembly, (b) exploded view of the top LCP (image courtesy of BOYD™), (c) cooler volume after integrating the DSC.

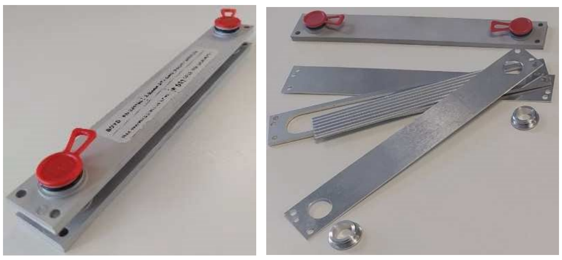

Fig. 3 Pictures of the fabricated cooler showing the complete cooler and the exploded view of the top LCP

However, in reality, the metal surfaces have a certain roughness and the TIM thickness actually varies from 0 (at the points where the metallic surfaces are actually in contact) to the maximum value (where the separation between the metals is the highest). This can be expected to cause some discrepancy between simulations and measurements (the simulations being the worst case, as far as the TIM is concerned). The thermal resistance is decomposed into different contributions, viz., that of the power module ($R_{\mathrm{th,jc}}$), that of the TIM ($R_{\mathrm{th,TIM}}$) and that of the cold plate ($R_{\mathrm{th,LCP}}$). For module-A, the temperature and pressure distributions are shown in Fig. 5. It can be seen from Fig. 5 (a) that chips of MOD3, which is the farthest from the fluid inlet, yield the highest temperature. This is because the fluid heats up during its course from the fluid inlet to outlet. Within a given module, the temperatures of the 4 chips are more-or-less similar, which indicates an optimal spatial separation of the chips on the substrate. From Fig. 5 (b) it can be seen that there are no critical hotspots on the substrate surface, confirming an optimal design of the module and cooler. Fig. 5 (c) shows a cross section of the system at the hottest chip, and Fig. 5 (d) shows the pressure drop. Fig. 5 (e) shows that the pressure drop of the cooling system, including the inlet and outlet manifolds, is 190 mbar, which is within the 200 mbar target.

Table 1 Boundary conditions for CFD simulations

Coolant	Water-Glycol (50:50) Density: 1082 kg/m3 Specific heat: 3300 J/kg-K Conductivity: 0.4 W/m-K Viscosity: 0.0046 kg/m-s Inlet Fluid Temperature, T_f=65°C Flow rate: 10 L/min, shared by the two LCPs
Power Module	3X DSC half bridge modules (i.e., 2x switches) Module-A: 48 mm2 chips per switch Module-B: 108 mm2 chips per switch
Dissipated Power Per switch¹	Module-A: P_{loss} = 300 W Module-B: P_{loss} = 441 W
TIM	4 W/m-K, 15 µm
Target Pressure Drop	200 mbar (typical automotive systems)

¹ Dissipated power is adjusted such as to reach T_{vj}=150°C.

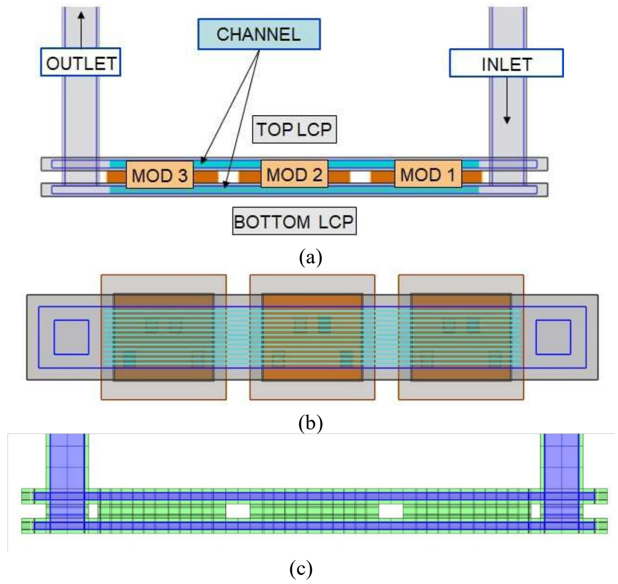

Fig. 4 Simulated geometry showing, (a) side view, (b) top view, (c) Hexahedral mesh – Solid regions in green, fluid regions in blue

The simulated intermediate temperatures and thermal resistances (along with their definitions) are recorded in Table *2*. It can be noted that the heat flow to the top and to the bottom is not symmetrical, due to the presence of spacers in the top path [1]. Module-A with the lower chip content has a ratio ~30:70 between top-bottom, whereas module-B with higher chip content has ~40:60. This is because module-B, owing to a higher chip content, has a higher contact area to the top substrate, resulting in a better heat flow to the top and, therefore, a better utilization of the module stack. Fig. 6 shows the split-up of the $R_{\mathrm{th,jf,top}}$ and $R_{\mathrm{th,jf,bot}}$ for both the modules. A significant contribution to both the top and bottom resistances is from the LCP and the TIM, whereas the module contributes only a small portion, especially on the bottom side (<25%). This also confirms the earlier made statement that optimizing the cooler and TIM plays a major role for high performance DSC modules.

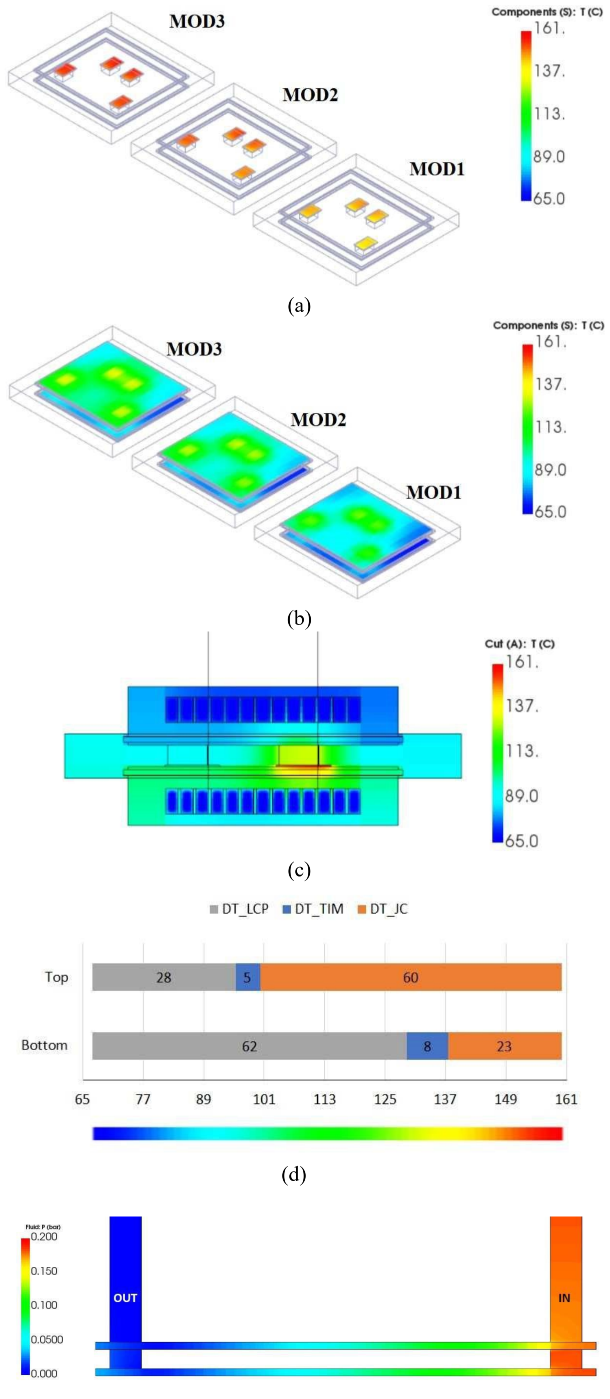

Fig. 5 Results of the CFD thermal simulations showing, (a) temperature maps of the chips, (b) temperature maps of the substrates, (c) a cross section of the system at the hottest chip, (d) Split-up of the temperature delta DT from fluid temperature to maximum chip temperature on both sides, (e) pressure drop of the cooling system.

Overall, module-A achieves an $R_{th,jf}$ = 0.28 K/W whereas module-B reaches $R_{th,jf}$ = 0.19 K/W which is impressive considering the size/volume of the cooler. Further optimization is possible, e.g., by simply increasing the size of the cooler, or by having a higher flow rate on the bottom than on the top, or by having a serial flow of the coolant such that it flows through the bottom LCP first, and then through the top LCP. These aspects will be considered in a future study.

Table 2 Summary of CFD simulation results: temperatures, thermal resistances (per switch) definitions and values

	Module-A	Module-B
Ratio of power flow to the top versus bottom, i.e., $P_{loss,top}$:$P_{loss,bot}$ in [W] in [%]	85:215 28:72	169:272 38:62
Chip average-temperature, T_{vj}	150.3 °C	151.1 °C
Module case[1] temperature: Top, $T_{c,top}$	79.6 °C	116.3 °C
Module case[1] temperature: Bottom, $T_{c,bot}$	101 °C	143.9 °C
LCP surface[1] temperature: Top, $T_{LCP,top}$	95.4 °C	111.6 °C
LCP surface[1] temperature: Bottom, $T_{LCP,bot}$	129.4 °C	136.9 °C
Thermal resistance junction to case		
$R_{th,jc,top} = (T_{vj} - T_{c,top})/P_{loss,top}$	0.58 K/W	0.21 K/W
$R_{th,jc,bot} = (T_{vj} - T_{c,bot})/P_{loss,bot}$	0.06 K/W	0.03 K/W
$R_{th,jc2} = (R_{th,jc,top} \parallel R_{th,jc,bot})$	0.05 K/W	0.02 K/W
Thermal resistance TIM		
$R_{th,TIM,top} = (T_{c,top} - T_{LCP,top}) / P_{loss,top}$	0.06 K/W	0.03 K/W
$R_{th,TIM,bot} = (T_{c,top} - T_{LCP,bot}) / P_{loss,bot}$	0.04 K/W	0.03 K/W
Thermal resistance LCP		
$R_{th,LCP,top} = (T_{LCP,top} - T_f) / P_{loss,top}$	0.36 K/W	0.28 K/W
$R_{th,LCP,bot} = (T_{LCP,bot} - T_f) / P_{loss,bot}$	0.30 K/W	0.26 K/W
Thermal resistance Junction-Fluid		
$R_{th,jf,top} = (T_{vj} - T_f) / P_{loss,top}$	0.99 K/W	0.51 K/W
$R_{th,jf,bot} = (T_{vj} - T_f) / P_{loss,bot}$	0.39 K/W	0.32 K/W
$R_{th,jf} = (T_{vj} - T_f) / P_{loss}$	0.28 K/W	0.19 K/W

[1]Measured on the surface, right below/above the center of the hottest chip.

[2]$R_{th,jc}$ is a virtual parameter and, unlike single side cooled modules, has no physical meaning.

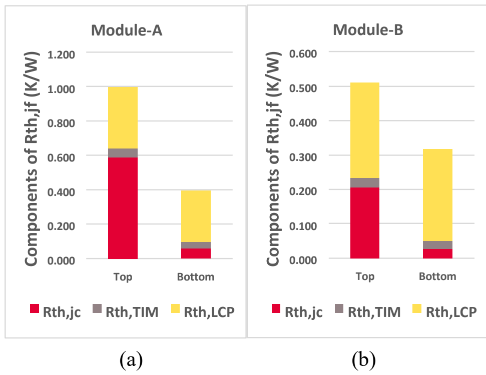

Fig. 6 Split-up of the simulated $R_{th,jf}$ for, (a) Module-A, (b) Module-B. Boundary conditions and definitions in Table 1.

B. Production Process- CAB Brazing Technology overview

The liquid cold plates are produced by the Controlled Atmosphere Brazing (CAB) process, a metallurgic welding process which allows the creation of a high-quality metal junction, as summarized in Fig. *7*. During the assembling process, foils of filler material are located in between the aluminum layers. These foils are made of a specific aluminum mixture able to melt at a temperature of approximately 600°C. Once the assembling process is completed, the structure is clamped in a custom designed brazing jig and inserted into a pre-warmed oven area. In order to avoid oxidation, the oxygen in the chamber atmosphere is substituted with nitrogen. This step of the procedure gives the name to the CAB process. Once the oven reaches an internal temperature of approximately 600°C, the foil material starts melting, while the aluminum layers are still in a solid stage. After the cooking, the pieces proceed to the cooling areas where they are progressively brought to ambient temperature. The CAB Brazing process requires a specific combination of aluminum alloy since the chemical composition of the materials is crucial to avoid micro-porosities along the brazing junction, which might cause leakage and consequently the failure of the LCPs during their operative life. For this reason, layers are made of Al3003, connectors of Al6060 and turbulators of Al1050.

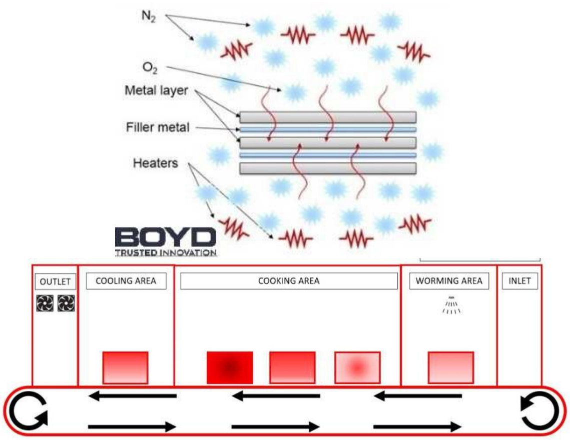

Fig. 7 Summary of the CAB Brazing fabrication process (image courtesy of BOYD™)

III. Experimental Characterization of DSC Module With a Lab-Cooler

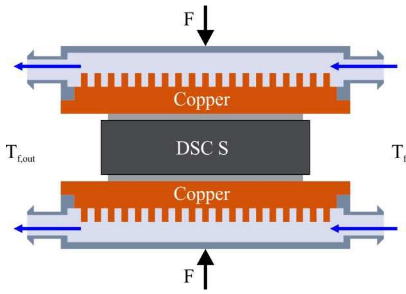

Fig. 8 Schematic representation of the experimental lab-setup for measuring the thermal characteristics of the DSC module.

The thermal performance of the DSC module is first characterized for a lab cooler (setup shown in Fig. 8), where the modules are placed with a defined orientation between two copper heatsinks with an internal pin-fin structure that is fluid cooled on both sides. In this case only module-A will be considered. A thermal interface material (TIM)- Dowsil TC5021 with a thermal conductivity of 3.3 W/mK and thickness of 50 µm is applied between the module and the heatsinks. A variable clamping force F of 400 N and 1000 N is applied between the upper and lower heatsinks structure with a springloaded holder to ensure a preset force, independent of thermomechanical influences during the test, which is also continuously controlled and ensured. A water-glycol-based fluid (50:50) recirculation unit with a regulated fluid flow rate between 4-10 L/min, a controlled fluid temperature of 60 °C is used to indirectly cool the modules. This setup allows choosing between parallel or serial fluid flow configurations. Fig. 8 shows the parallel fluid flow configuration, whereby both heat sinks are supplied with the same fluid stream in parallel (50:50 ratio). For the determination of the junction temperature T_{vj}, the characteristic curve of the internal body diode of the SiC MOSFET is first calibrated at different temperatures. A constant calibration current corresponding to 1/1000 of the nominal current is used for this purpose. Knowing the relationship between the body diode forward voltage and T_{vj}, the determination of R_{th} can now be applied. For the case of $R_{th,jf}$ measurement, a current heating pulse is applied to the ohmic drain-source channel of the DSC module until the system reaches a thermal steady-state. This pulse generates a thermal power injection, P_{loss}, in the semiconductor junction of the module according to Jouleheating. By means of precisely timed measurement of the junction temperature T_{vj} directly after switching off the current heating pulse, conclusions are drawn about T_{vj} in connection with P_{loss}. Finally by measuring T_f, $R_{th,jf}$ can be determined according to the equations in Table 2.

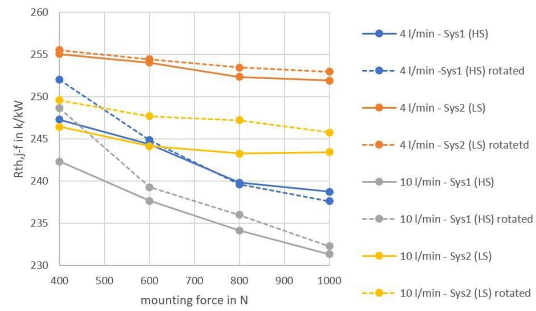

(a)

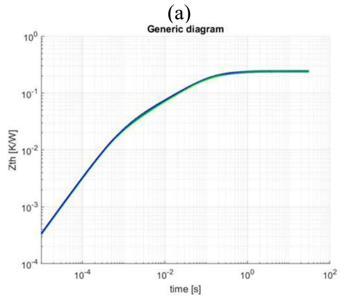

(b)

Fig. 9 (a) Measured values for DSC with the lab cooler showing (a) $R_{th,jf}$ as a function of applied clamping force F, (b) $Z_{th,jf}$ curve

Fig. 9 (a) shows the measured dependence of $R_{th,jf}$ on the applied clamping force F. Various module orientations (rotated and not rotated), different flow rates (4 and 10 L/min), application of the current heating pulse to the high-side (HS) MOSFET and the low side (LS) MOSFET of the half bridge are analyzed. The $R_{th,jf}$ for the investigated module shows a rather weak dependency on F. $R_{th,jf}$ is lower at higher fluid rates, due to the increased heat extraction. Furthermore, no significant dependence is observed with regard to the mounting orientation of the module. Rotated-suffix in Fig. 9(a) corresponds to a rotation of the module by 180° around one of the geometric main axes of the module. The rotatednon-rotated measurement results show a low variation in $R_{th,jf}$, indicating a good repeatability in the experimental setup. At F=1000 N and a fluid flow rate of 10 L/min, a value of $R_{th,jf}$ =
0.23 K/W is achieved. Compared to the simulation results (0.28 K/W), this is significantly lower. This is because, the lab cooler is made of copper (versus Aluminum), is larger than the BOYD™ cooler, and also due to the inaccuracies involved in modeling the TIM, mentioned earlier. Fig. 9 (b) shows the measured thermal impedance $Z_{th}(t)$, where it can

be seen that Z_{th} = 0.025 K/W at t = 1 ms. This corresponds to a tenth of the value at thermal equilibrium, $R_{th,jf}$. The module reaches thermal steady-state in ~1 s.

IV. Experimental Verification of BOYD™ Cooler

The BOYD™ cooler described previously is experimentally verified in the R_{th} measurement setup shown in the previous section (same setup and boundary conditions, except the cooler itself and the module which in this case is Module-B). TIM is first applied to the DSC modules on both sides, before mounting them on the cooler as seen in Fig. 10(a). A stencil is used to enable a uniform thickness of 50µm (before application of a clamping force). Two milled-aluminum threaded adaptors interface the cooler to the coolant circuit as shown in Fig. 10 (b). The current cooler design lacks the possibility to apply a given force from within itself (this is being implemented in an upcoming version). Therefore, a clamping structure including a force-gauge is fixed around the central area, to apply a known force (in this case 650N).

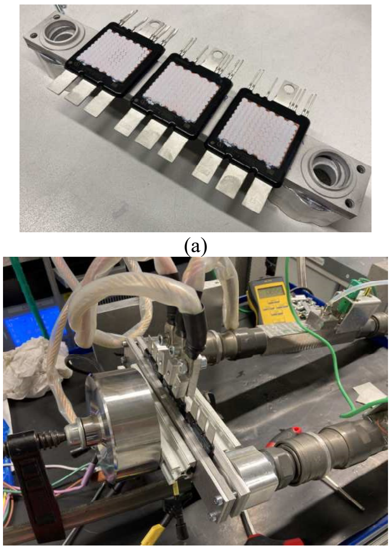

(a)

(b)

Fig. 10 Infineon's HybridPACK™ DSC prototypes integrated into the BOYD™ cooler, (a) Modules with TIM paste before applying top LCP, (b) Experimental setup for characterization of $R_{th,jf}$

Fig. 11(a) shows the measured $R_{th,jf}$ and the corresponding pressure drop for the high-side (HS) and low-side (LS) switches for different flow rates (6, 10 and 16 L/min). As can be expected, higher flow rate improves the $R_{th,jf}$ and it can be seen that $R_{th,jf}$ decreases by about 5% with every 5 L/min increment. Furthermore, it appears that the HS switch has a worse $R_{th,jf}$ than the LS switch. This is partially caused by the different locations of the chips inside the modules and their mutual heating. Please note, however, that this may also be attributed to a combination of several other factors such as spreads in the chip/module- and cooler production, variance in efficacy of the TIM layer over the module and distribution of the applied force, and may not be generalized. At 10 L/min, a typical flow rate for automotive inverters, an $R_{th,jf}$ of 0.18 K/W (average of HS and LS) is measured. Again, this is lower compared to the simulated value (0.19 K/W) and this is mainly due to the modelling of the TIM as explained earlier. For a battery voltage of 400V, $R_{th,jf}$ of 0.18 K/W would mean that module-B can handle a continuous I_{RMS} > 450A or power > 150kW. This would translate into a volumetric power density (considering just the cooler and the module) of > 375 kW/L. Fig. 11(b) depicts the measured $Z_{th}(t)$ for a coolant flow rate of 10 L/min. At time value of 1 ms, Z_{th} corresponds to a value of about 0.011 K/W and steady state is achieved in < 5 s.

Compared to the lab-cooler (~1 s), the BOYD™ cooler takes longer to reach steady-state, which restricts T_{vj} during transient events (e.g., short acceleration/braking).

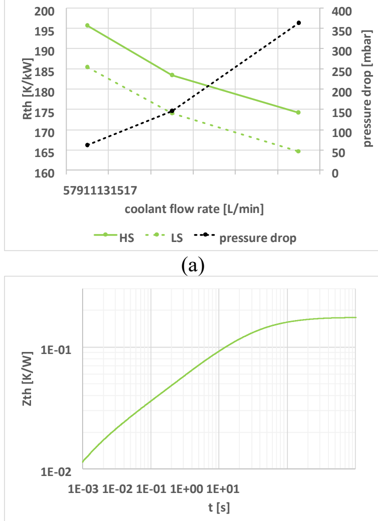

(a)

(b)

Fig. 11 Experimental results showing, (a) the measured $R_{th,jf}$ for the HS and LS switches as a function of flow rate, (c) $Z_{th,jf}$ curve, for the DSC with the BOYD™ cooler

V. Si-IGBT versus SiC-MOSFET in a DSC Package

This section compares a Silicon (Si) IGBT-based DSC module versus a SiC MOSFET-based DSC module. For a fair comparison [2] [3] [4] [5] [6], both modules chosen are such that they roughly cater to an RMS current of 400A at a battery voltage of 400V (details of the compared modules are in [1]). The static and switching performance of both modules are experimentally measured and compared in Fig. 12. The gate resistances for both devices are tuned to keep dv/dt <= 10 kV/µs and the voltage overshoot below the breakdown voltage, to reflect application-near conditions. It can be confirmed that the voltage drop of the MOSFET, V_{ds}, is significantly lower than that of the IGBT, V_{ce}, at light load due to the resistive nature of the MOSFET compared to the kneelike voltage behavior of the IGBT [2]. From the switching characteristics, it can be confirmed that the diode recovery losses E_{rec} in the SiC MOSFET are only an eighth of that in the IGBT. This is because, minority charge carriers have a significantly lower lifetime in the SiC Body diode compared to the Si FWD, resulting in a quicker extraction of charges during diode turn-off. The benefits of reverse recovery also reflect on the turn-on losses E_{on}, where it can be seen that the SiC module has a factor 3 lower losses than the Si module. The turn-off losses E_{off} in the SiC Module are lower by ~30% than the IGBT module, due to the absence of tail currents (which is again a bipolar phenomenon, relating to the decay of minority charge carriers). These measurements confirm the benefits of the SiC Module. In order to check the benefits of the SiC Module at the inverter level, power loss simulations are carried out for the Worldwide Harmonized Light Vehicle Test Procedure (WLTP), which is a commonly used mission profile for benchmarking automobiles [2], as shown in Fig. 13. The boundary conditions can be found in [1]. The observations in the previous paragraph can be confirmed. The conduction losses in the SiC MOSFET are lower than the Si-IGBT by

>75%, whereas the corresponding reduction in the switching losses is >60%.

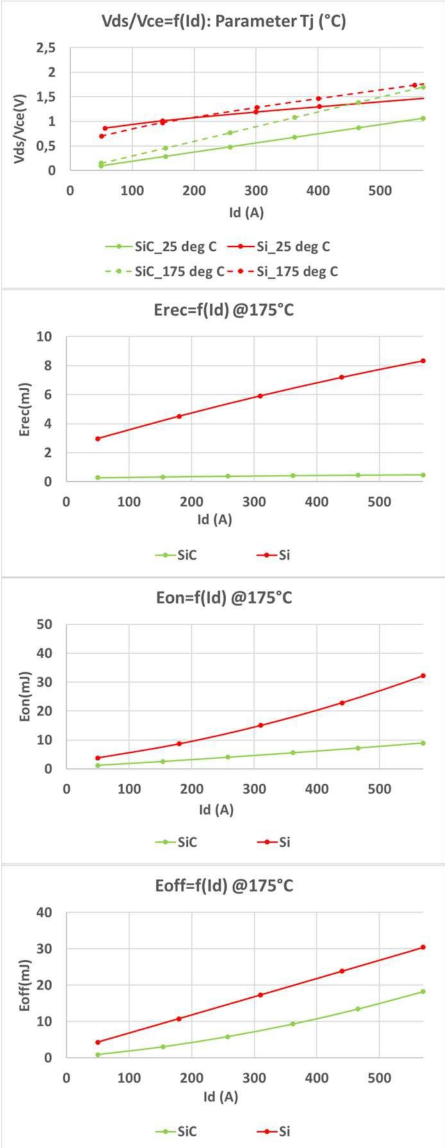

Fig. 12 Measured Static and dynamic characteristics of the DSC SiC versus DSC- Si at V_{dc} = 400 V, R_g (SiC) = 5.1 Ω, V_{gs} (SiC) = 18 V, R_g (Si) = 3.6 Ω, V_{gs} (Si) = 15V.

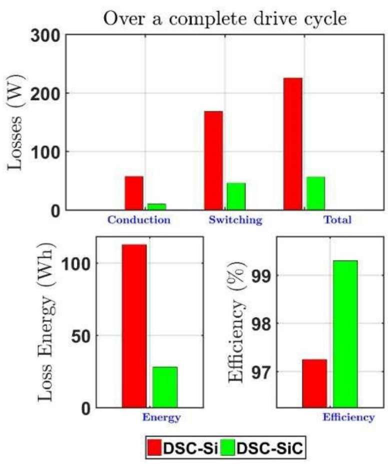

Fig. 13 Simulated power losses for DSC Si and DSC SiC for the WLTP Mission profile of a mid-sized sedan similar to a Volkswagen e-golf. Boundary conditions: V_{dc} = 400 V, f_{sw} = 10 kHz [1]

As a whole, the average power losses in the SiC Module are 60% lower than the Si module, resulting in an improvement of the inverter efficiency by over 2 percentage points, compared to the Si module. This re-affirms the efficiency benefits of the DSC SiC Module.

VI. Conclusions and Future Work

This paper presented the HybridPACK™ DSC Power Module based on CoolSiC™ Trench SiC MOSFETs, suitable for high performance automotive traction inverter applications. A compact Aluminum-based cooler was designed for DSC, and CFD thermal- and hydraulic simulations were performed to analyze its performance. The volume of the cooler together with the modules was calculated to only 0.4 L. It was shown that the contribution of the power module to the thermal resistance was low. The ratio of heat extraction from top to bottom was 30:70 for moduleA (with 48 mm2 chips per switch), but this increased to 40:60 for module-B (with 108 mm2 chips per switch), indicating a better utilization of the thermal stack for larger chip content. Overall, the modules achieved an $R_{th,jf}$ of 0.28 K/W and 0.19 K/W respectively, at 10 L/min flow. To experimentally verify the simulations, the DSC modules were characterized- module-A with a lab cooler and module-B with the BOYD™ cooler. As expected, the measured $R_{th,jf}$ were lower than simulations due to the inaccuracies in simulating the TIM. At 10 L/min flow rate, module-A achieved $R_{th,jf}$ = 0.23 K/W with the lab cooler, whereas module-B achieved $R_{th,jf}$ = 0.18 K/W. For a battery voltage of 400 V, this translates into a continuous I_{RMS} over > 450 A and power > 150 kW. This results in an impressive volumetric power density (considering just the cooler and the module) of > 375 kW/L.

Future Work: Work is ongoing to further optimize the cooler and to design clamping structures within the cooler to apply pre-defined force on the modules for a good contact. Also, measurements are ongoing with various TIM available in the market, to determine the most suitable TIM for the DSC.

References

[1] A. P. Pai, M. Ebli, T. Simmet, A. Lis and M. Beninger-Bina, "Characteristics of a SiC MOSFET-based Double Side Cooled High Performance Power Module for Automotive Traction Inverter Applications," *IEEE/AIAA Transportation Electrification Conference and Electric Aircraft Technologies Symposium,* 2022.

[2] A. P. Pai, Impact of Silicon Carbide based Power Modules on Mission Profile Efficiency of Automotive Traction Inverters, Shaker, 2020.

[3] A. P. Pai, T. Reiter and M. Maerz, "A new behavioral model for accurate loss calculations in power semiconductors," in *PCIM Europe 2016; International Exhibition and Conference for Power Electronics, Intelligent Motion, Renewable Energy and Energy Management*, 2016.

[4] A. P. Pai, T. Reiter and M. Maerz, "An improved behavioral model for loss calculations in automotive inverters," in *EEHE 2016 Wiesloch; Proceedings of*, 2016.

[5] A. P. Pai, T. Reiter, O. Vodyakho and M. Maerz, "Mission Profile Analysis of a SiC Hybrid Module for Automotive Traction Inverters and its Experimental Power-loss Validation with Electrical and Calorimetric Methods," ASTES Journal, vol. 3, 2018.

[6] A. P. Pai, T. Reiter, O. Vodyakho, I. Yoo and M. Maerz, "A calorimetrie method for measuring power losses in power semiconductor modules," in *2017 19th European Conference on Power Electronics and Applications (EPE'17 ECCE Europe),* 2017.